Article:
Caudwell, JA orcid.org/0000-0002-0199-1585, Tinkler, JM orcid.org/0000-0002-6098-4908, Johnson, BRG orcid.org/0000-0001-9715-1160 et al. (8 more authors) (2022) Protein-conjugated microbubbles for the selective targeting of S. aureus biofilms. Biofilm, 4. 100074. ISSN 2590-2075

https://doi.org/10.1016/j.bioflm.2022.100074

Biofilm 4 (2022) 100074

Contents lists available at ScienceDirect

Biofilm

journal homepage: www.sciencedirect.com/journal/biofilm

Protein-conjugated microbubbles for the selective targeting of *S. aureus* biofilms

Jack A. Caudwell [a,b,c,1], Jordan M. Tinkler [d,1], Ben R.G. Johnson [d], Kenneth J. McDowall [b,e], Fayez Alsulaimani [b,e], Christian Tiede [e,i], Darren C. Tomlinson [b,e,f], Steven Freear [g], W. Bruce Turnbull [b,c], Stephen D. Evans [b,d], Jonathan A.T. Sandoe [a,h,*]

[a] School of Medicine and Health, University of Leeds, Leeds, UK
[b] Astbury Centre for Structural Molecular Biology, University of Leeds, Leeds, UK
[c] School of Chemistry, University of Leeds, Leeds, UK
[d] School of Physics and Astronomy, University of Leeds, Leeds, UK
[e] School of Molecular and Cellular Biology, University of Leeds, UK
[f] Biomedical Health Research Centre, Bioscreening Technology Group, University of Leeds, Leeds, UK
[g] School of Electronic and Electrical Engineering, University of Leeds, Leeds, UK
[h] Leeds Teaching Hospitals NHS Trust Leeds, Leeds, UK
[i] BioScreening Technology Group, Faculty of Biological Sciences, University of Leeds, Leeds, UK

ARTICLE INFO

Keywords:
Ultrasound contrast agents
Biofilm
Staphylococcus aureus
Molecular targeting
Affimer protein
Sonobactericide
Ultrasound

ABSTRACT

Staphylococcus aureus (*S. aureus*) is an important human pathogen and a common cause of bloodstream infection. The ability of *S. aureus* to form biofilms, particularly on medical devices, makes treatment difficult, as does its tendency to spread within the body and cause secondary foci of infection. Prolonged courses of intravenous antimicrobial treatment are usually required for serious *S. aureus* infections. This work investigates the *in vitro* attachment of microbubbles to *S. aureus* biofilms via a novel Affimer protein, AClfA1, which targets the clumping factor A (ClfA) virulence factor – a cell-wall anchored protein associated with surface attachment. Microbubbles (MBs) are micron-sized gas-filled bubbles encapsulated by a lipid, polymer, or protein monolayer or other surfactant-based material. Affimers are small (~12 kDa) heat-stable binding proteins developed as replacements for antibodies. The binding kinetics of AClfA1 against *S. aureus* ClfA showed strong binding affinity ($K_D = 62 \pm 3$ nM). AClfA1 was then shown to bind *S. aureus* biofilms under flow conditions both as a free ligand and when bound to microparticles (polymer beads or microbubbles). Microbubbles functionalized with AClfA1 demonstrated an 8-fold increase in binding compared to microbubbles functionalized with an identical Affimer scaffold but lacking the recognition groups. Bound MBs were able to withstand flow rates of 250 μL/min. Finally, ultrasound was applied to burst the biofilm bound MBs to determine whether this would lead to biofilm biomass loss or cell death. Application of a 2.25 MHz ultrasound profile (with a peak negative pressure of 0.8 MPa and consisting of a 22-cycle sine wave, at a pulse repetition rate of 10 kHz) for 2 s to a biofilm decorated with targeted MBs, led to a 25% increase in biomass loss and a concomitant 8% increase in dead cell count. The results of this work show that Affimers can be developed to target *S. aureus* biofilms and that such Affimers can be attached to contrast agents such as microbubbles or polymer beads and offer potential, with some optimization, for drug-free biofilm treatment.

1. Introduction

Staphylococcus aureus (*S. aureus)* is a common pathogen, frequently associated with the formation of biofilms in intravascular catheters or organs within the body. It is one of the most serious causes of bloodstream infection with mortality rates of 17–45.7%, and causes approximately 12,700 and 119,000 cases per year in England and the United States of America, respectively [1–5]. Bacteria are known to exist in three common states; planktonic, non-surface attached aggregates, and

* Corresponding author. School of Medicine and Health, University of Leeds, Leeds, UK
E-mail address: j.sandoe@leeds.ac.uk (J.A.T. Sandoe).
[1] indicates joint first author.

https://doi.org/10.1016/j.biofilm.2022.100074
Received 17 November 2021; Received in revised form 1 March 2022; Accepted 6 March 2022
Available online 19 March 2022

Abbreviations

MB(s)	microbubble(s)
ClfA	Clumping Factor A
US	Ultrasound
UCA(s)	ultrasound contrast agent(s)
A647	Alexa Fluor 647
AAC	Affimer-Alanine-Cystatin.

surface-attached biofilms [6]. Surface-attached biofilms are agglomerations of microbes, in a range of growth and metabolic states, together with a matrix of secreted proteins, carbohydrates, extracellular DNA (eDNA), and "scavenged" host molecules [4,7]. The formation of biofilms on medical devices such as intravascular catheters, cardiac pacemakers and prosthetic joints makes infection difficult to eradicate with antimicrobial therapy alone and frequently requires removal of the device [4,8]. Treatment failure in the context of biofilm infections is multifactorial but partly explained by the 100–1000 fold decrease in antibiotic susceptibility of bacteria in biofilms when compared with their planktonic counterparts [9–11]. Patients with *S. aureus* bloodstream infections require extensive investigation to determine the source of infection, which can be challenging, not least because of the tendency of *S. aureus* to spread and cause secondary foci of infection within the body. Echocardiography is a routine part of the investigation of *S. aureus* bloodstream infection because of the frequency of endocardial involvement and the difficulty confirming a diagnosis of infective endocarditis [12,13]. Prolonged courses of intravenous antimicrobial treatment are usually required for these serious *S. aureus* infections.

Microbubbles (MBs) are micron-sized gas-filled bubbles encapsulated by a lipid monolayer or other surfactant-based material [14,15]. MBs have been engineered to be used as ultrasound contrast agents (UCAs) and are in routine clinical use, for example during the echocardiographic examination of cardiac blood flow. Clinically approved MBs such as Definity® and SonoVue have mean diameters between 1 and 3 μm allowing flow through the vasculature [16–20].

Microbubbles have been targeted against tumour vasculature using BR55, VEGFR1/2, CD-31, PD-L1, FSHR, $\alpha_v\beta_3$ integrin targets, and other relevant targets [21–33]. Most studies have focused on using targeting to aid the identification of tumors through enhanced ultrasound imaging, with improved therapeutic delivery of chemotherapeutic agents also demonstrated [26]. Targeted MBs have also been utilized as a non-invasive method of assessing inflammation sites by targeting activated leukocytes [34–36]. Finally, alternative strategies for achieving microbubble localization have been developed which involve the incorporation of magnetic nanoparticles within the MB shell [37–39]. The use of an external magnet causes the accumulation of MBs at the desired site.

Targeting of MBs in the context of human infection has seen comparatively little research interest within the same time frame and only two such examples have been identified. *Matter* et al. demonstrated the synergy of MBs and targeted monoclonal antibodies (mAbs) as a novel method of non-invasive high-frequency ultrasound imaging of biofilms for structural investigations [40]. The second study involved the integration of vancomycin, a commonly used antibiotic, into the shell of MBs for the targeting of *S. aureus* biofilms [41].

Non-targeted treatment approaches combining MBs and US have demonstrated the ability to kill bacteria and remove biofilm [42–44]. It has been demonstrated that MBs can be used as a method for disrupting biofilms *in vitro*. For example, *Lattwein* et al. used a combination treatment comprised of MBs, ultrasound and oxacillin to treat an *in vitro* model of a blood clot-associated *S. aureus* biofilm [45]. They found that the combination treatment achieved greater efficacy for biofilm remediation than either treatment alone.

Affimers are small (~12 kDa), heat-stable binding proteins that are being developed as replacements for antibodies (~150 kDa) for a wide variety of applications [46]. Affimer proteins, as shown in Fig. 1, have a conserved cystatin scaffold (blue) and two hypervariable loops (purple), the amino acid sequence of which dictates the affinity of an Affimer to its desired target. In addition, due to their smaller size, Affimers tend to be more structurally stable than their antibody counterparts.

In this study we first determined the binding efficacy of the Affimer AClfA1 using a combination of isothermal titration calorimetry and surface plasmon resonance. AClfA1 targets clumping factor A (ClfA) a cell wall bound virulence factor located on the surface of *S. aureus* cells. ClfA is one of several cell wall-anchored virulence factors that is associated with cell-surface attachment interactions that aid early colonization by bacterial cells and enables the development of biofilms [48–51]. The AClfA1 Affimer was compared against a control Affimer, Affimer Alanine Cystatin (AAC) which was identical except for removal of the active targeting peptide sequence. We subsequently attached the Affimer to polymer beads and microbubbles, using the NTA/his-tag chemistry, and then determined the efficacy of binding the Affimer labelled polymer particles and microbubbles to a *S. aureus* biofilm, grown in a microfluidic platform, using a combination of confocal

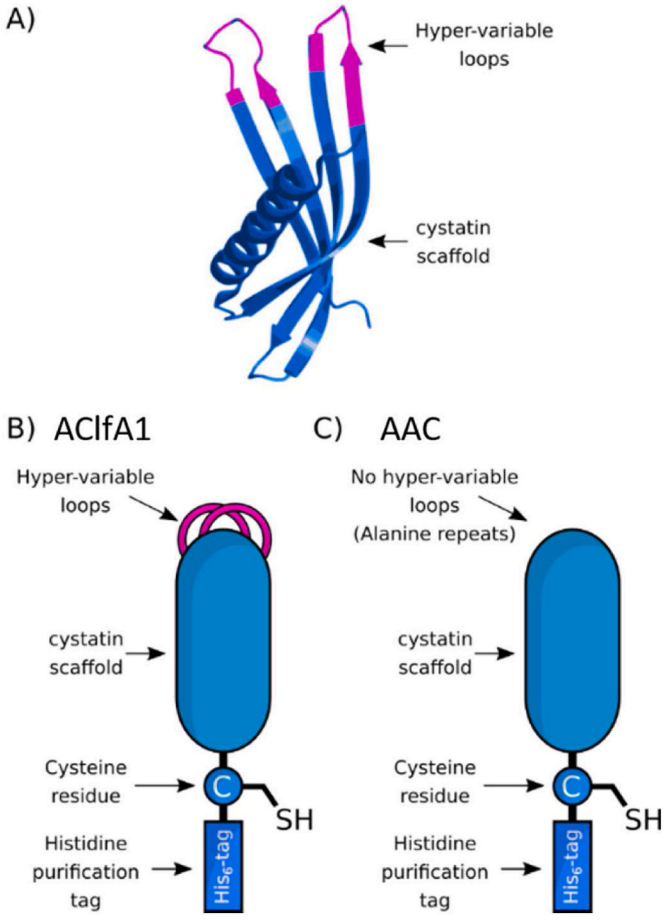

Fig. 1. A) Crystal structure of the general Affimer protein construct [47]. B) Cartoon representation of the Affimer ClfA1 (AClfA1), with the hypervariable loop binding site in pink and conserved cystatin scaffold in blue. C) Cartoon representation of the Affimer protein, Affimer Alanine Cystatin (AAC), was used as a control containing a series of alanine repeats in the hypervariable loop sections to prevent specific binding but maintain the cystatin scaffold structure. Both proteins have a poly-histidine tag for purification and bead conjugation, and a cysteine residue for MB conjugation. (For interpretation of the references to colour in this figure legend, the reader is referred to the Web version of this article.)

fluorescence laser scanning microscopy (CLSM) and bright field imaging.

2. Materials and methods

2.1. Microfluidic platform for biofilm studies

Microfluidic devices (Fig. 2A, Figure SI1) similar to those used by Paquet-Mercier et al. were used for biofilm cultivation and subsequent Affimer protein binding studies [52]. Each device contained three chambers, which could be exposed to different control or experimental conditions. Microfluidic devices were fabricated using standard photo- and soft-lithographic techniques. A 3-inch diameter silicon wafer (PI-KEM Ltd, Tamworth, UK) was initially cleaned using acetone, isopropanol, distilled water, and then dried. A layer of SU8-2075 (Microchem, Warwickshire, UK) was spin-coated onto the wafer to a height of 180 μm. Designs were then written in the SU8 layer using a 375 nm laser (MicroWriter ML, Durham Magneto-Optics, Durham, UK). Devices were cast from the SU8/silicon master in polydimethylsiloxane (PDMS) using a 1:10 ratio of the cross-linker to polymer base (Sylgard 184, Dow Inc, Midland, MI, USA). The PDMS was left under vacuum for 30 min to remove air bubbles and placed in an oven at 75 °C for 1 h to set. Individual devices were then cut, hole punched, and bound to #1.5H 24 × 50 mm glass coverslips (Thorlabs Inc, Newton, NJ, USA) using oxygen plasma treatment (Zepto, Diener, Ebhausen, Germany). Modelling of the devices using flow rates of 80–250 μL/min predicted that the chamber flow velocities would cause fluid shear forces of the order 0.023–0.072 Nm^{-2}.

2.2. Microfluidic biofilm cultivation

Microfluidic components were sterilized in a vacuum autoclave (Sun 23L Class B, MingTai, Ningbo, China) at 121 °C for 20 min, the microfluidic device was then assembled and exposed to UV for 30 min and rinsed with 70% ethanol and allowed to dry. The system (Figure SI2) was equilibrated with autoclaved brain heart infusion broth (BHI, Sigma-Aldrich, St Louis, MO, USA). The microfluidic device was pre-treated with 0.22 μm syringe filtered human fibrinogen (5 mg mL^{-1}, Sigma-Aldrich, St Louis, MO, USA) to promote bacterial adhesion to microfluidic chamber surfaces [53,54]. System sterility was ascertained before bacterial inoculation by plating out BHI broth previously flowed through the system, onto horse blood agar (Thermo Fisher Scientific, Waltham, MA, USA). The microfluidic device was seeded with an overnight culture of UAMS-1 *S. aureus* cells at a concentration of the order 10^9 CFU mL^{-1} and left static for 2 h at 37 °C to allow bacterial adhesion. BHI media was then flowed through the chambers at ~ 80 μL/min for 24 h, at 37 °C. Biofilms were maintained at 37 °C during growth, staining, and imaging aspects of experimental work. The attachment of beads/MBs and the application of US were carried out at room temperature because the device had to be removed from the heated stage of the microscope, this process took ~10 min.

2.3. Fluorescent staining and biofilm imaging

The cultured biofilms were stained using a LIVE/DEAD cell viability kit (Biotium Inc, Fremont, CA, USA) containing DMAO™ for bead and MB attachment proof of concept work. The stain kit was changed to SYTO™ 9 and Propidium Iodide (PI) (BacLight, Invitrogen, Thermo Fisher, MA, USA), which was found to provide more reliable viability data. The former stain kit was used in tMB attachment studies by combining 5 mM DMAO™ with 1 mL of 0.22 μm filtered 150 mM NaCl solution a 1:8 ratio, this was then diluted to 1 mL and vortexed before use. For cell viability assessment, 1.5 μL of 20 mM PI and 3.34 μM SYTO™ 9 were added to 1 mL of 0.22 μm filtered 0.85% NaCl solution and vortexed before use. Biofilms were incubated with the relevant stain for 20 min. Once stained, the microfluidic device was mounted onto a confocal laser scanning microscope (CLSM) (SP8, Leica, Wetzlar, Germany). Fig. 2B shows the CLSM imaging setup applied using a 100 × oil immersion objective (HC PL APO CS2 FWD 0.13 mm NA 1.4).

2.4. Selection of anti-clumping factor A Affimer (AClfA1) proteins

Recombinantly produced ClfA/ySUMO fusion protein and ySUMO protein were biotinylated using EZ-Link NHS-biotin (Cat. No. 20217, ThermoFisher Scientific, Waltham, MA, USA). In brief, for 100 μL of a 12.5 μM solution of ClfA/ySUMO fusion protein, 0.8 μL of 10 mM EZ-Link NHS-Biotin reagent was added and incubated for 30min at room temperature. Excess biotin was subsequently removed using Zeba Spin

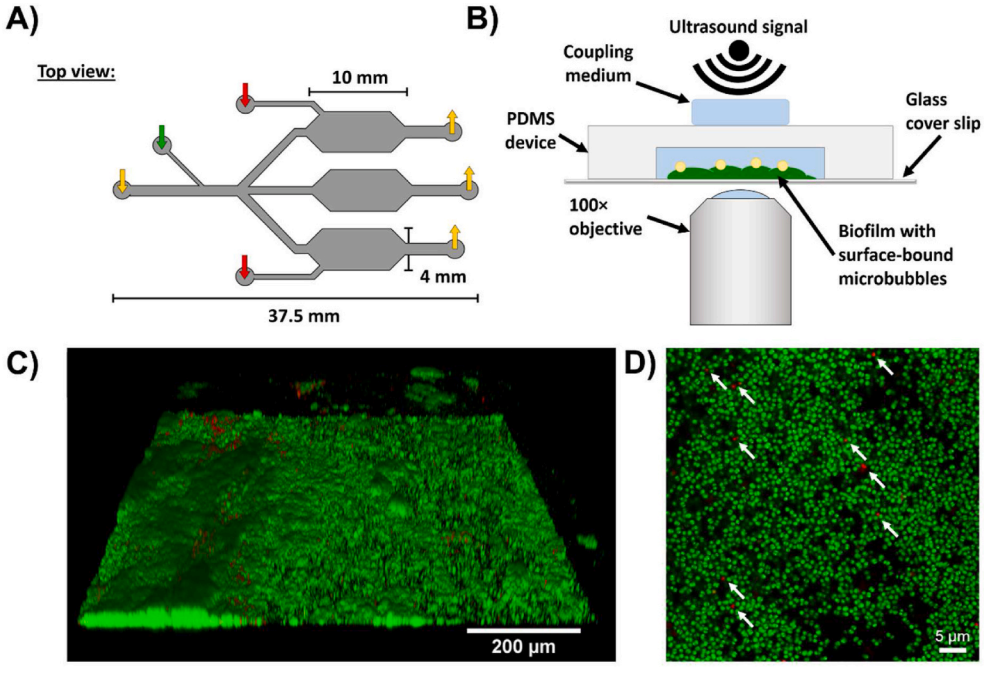

Fig. 2. A) Schematic of microfluidic flow chip used for biofilm growth. Coloured arrows indicate the direction of flow with yellow showing primary media inlet and outlets, green showing inoculum inlet, and red showing reagent inlets. Black scale bars indicate chamber dimensions, more comprehensive schematics of the devices used are included in the supplementary information (Figure SI1). B) Schematic of the experimental setup in the orientation used for ultrasound exposure and confocal laser scanning microscopy (CLSM) imaging. C) Top-side view of a 3D rendered CLSM Z-stack image series obtained using CLSM and a 10 × objective showing lawn-like and 3D biofilm growth. Biofilms were stained using SYTO™ 9 (live + dead, green) and propidium iodide (dead, red). D) A high resolution, single plane, CLSM image obtained using a 100× objective on the top layer of biofilm growth. White arrows have been added to highlight locations of dead cells within the imaging area. (For interpretation of the references to colour in this figure legend, the reader is referred to the Web version of this article.)

desalting columns, 7 K MWCO (Cat. No. 89882/89883, ThermoFisher Scientific, Waltham, MA, USA). Phage display screening was performed with stringent negative selection against ySUMO protein as previously described with one alteration [55]. In contrast to the published protocol, the negative selection was also performed in the first panning round by immobilizing the pre-pan wells with 1 μg of biotinylated ySUMO protein prior to the incubation with the Affimer phage library. After three rounds of panning randomly selected clones were tested for binding ClfA by phage ELISA as previously described (Figure SI3) [56]. ClfA was prepared as outlined in section 4 of the supplementary information.

2.5. Production of Affimer proteins AClfA1 and AAC

The binding ability of AClfA1 was compared to a non-binding Affimer scaffold (AAC) control in which the hypervariable loops had been replaced with alanine repeats (Fig. 1C). Affimer proteins were prepared as described in section 4 of the supplementary information. Plasmids containing the vector for AClfA1 protein expression were transferred into BL21 GOLD DE3 *E. coli* cells. Protein expression was induced by using auto-induction media. Proteins were isolated from the cell lysate using nickel affinity chromatography. The Affimer proteins used for targeting microbeads and MB against biofilms were tagged with Alexa Fluor 647 to aid visualization during CLSM imaging. Alexa Fluor 647 NHS Ester (ThermoFisher, Waltham, MA, USA) was covalently attached to N-terminal amines and primary amine groups associated with lysine residues.

2.6. Isothermal titration calorimetry (ITC)

The interaction between ClfA and AClfA1 was studied using isothermal titration calorimetry (ITC) (MicroCal, Malvern Panalytical, Malvern, UK). AClfA1 and the AAC control were dialyzed into phosphate buffer (50 mM Na_2HPO_4/NaH_2PO_4, 150 mM NaCl, pH 7.4). The protein was concentrated by centrifugal concentration (Amicon 10 kDa MWCO). ITC binding assays were performed using a Microcal iTC200 (GE), at 25 °C. The AClfA1 sample was loaded into the sample cell (200 μL, 20 μM) and the Affimer titrant was loaded into the sample syringe (70 μL, 200 μM). Each titration experiment consisted of a sacrificial injection of 0.4 μL followed by 19 injections of 2 μL. Titration data were analyzed using a one-site binding model in Origin 7 software [57]. ClfA was prepared as outlined in section 3 of the supplementary information.

2.7. Polystyrene bead – Affimer conjugation

A known volume of 2 μm diameter Nickel (II) nitrilotriacetic acid (NTA) polystyrene beads (10^9 beads mL^{-1}) (micromod Partikeltechnologie GmbH, Rostock, Germany) were pelleted using centrifugation (13,000 × *g*, 2 min) in a 1.5 mL Eppendorf tube. The water storage solution was removed, and the beads resuspended in phosphate buffer (50 mM Na_2HPO_4/NaH_2PO_4, 150 mM NaCl, pH 7.4) to the original concentration. The beads were then pelleted by ultracentrifugation (13,000×*g*, 4 min) and resuspended in 10 μM of AClfA1 protein, in phosphate buffer, to give the original bead concentration. The presence of a His-tag on the Affimer protein was essential for conjugation. Protein samples were incubated at room temperature for 3–4 h at a low shake rate, fluorescently labelled samples were wrapped in foil to prevent photobleaching. The beads were then pelleted and the supernatant containing unbound protein removed, and the beads resuspended in buffer. Decanting and resuspension steps were repeated twice to wash beads of unconjugated protein, beads were diluted to a final concentration of 10^8 beads mL^{-1} for biofilm attachment studies.

2.8. Lipid preparation

MBs were prepared from a 95:5 M ratio of dipalmitoylphosphatidylcholine (DPPC) (Lipoid, Ludwigshafen, Germany) and 1,2-distearoyl-*sn*-glycero-3-phosphoethanolamine-N-[maleimide(polyethylene glycol)-2000] (DSPE–PEG2000–Maleimide) (Avanti Polar Lipids, Alabaster, AL, USA). The lipids, initially dissolved in a 50:50 chloroform and methanol mixture, were dried on the walls of a glass vial under nitrogen for 40 min. This was followed by overnight vacuum desiccation to remove any remaining solvent in the lipid sample. The lipids were resuspended in 0.22 μm filtered solution of PBS 1% glycerol (vol/vol) to a final concentration of 2 mg mL^{-1}. Prior to MB production, 10 μL of tetradecafluorohexane (C_6F_{14}) (Sigma-Aldrich, St. Louis, Mo, USA) per 1 mL of lipid solution was added to improve stability and MB lifetime [58].

2.9. Microbubble production and sample quantification

MBs containing DPPC and DSPE–PEG2000–Maleimide (95:5) were produced using a multiplexed microfluidic microspray device, previously described [59]. The lipid solution was introduced at a flow rate of 90 μL min^{-1} and combined with a decafluorobutane (C_4F_{10}) gas stream using a pressure of 1100 mbar. Following production, samples were removed and diluted 10 × in PBS for optical microscopy with a 40 × objective (90i, Nikon, Japan) performed using a 50 μm observation chamber. MATLAB (The Mathworks Inc, Natick, MA, USA) was used to analyze the MB samples and obtain sizing and concentration data [60].

2.10. Microbubble – Affimer attachment and washing

Both AAC and AClfA1 were attached to the surface of the lipid-shelled MBs via a maleimide-thiol linkage (Michael reaction). A free thiol group was present in the cystatin scaffold of both Affimer proteins (shown in Fig. 1B and C), and maleimide-labelled lipids were incorporated into the MB shell. Following production and initial imaging of MBs, Alexa Fluor 647 tagged AClfA1 and AAC, both maintained in PBS (pH 7.4), were added to separate MB samples, mixed gently, and incubated at room temperature for 30 min to allow binding. The volume of 7.5 μM Affimer required for each sample was calculated based on the number of MBs in each sample and the maximum packing efficiency of the Affimer. The excess of fluorescently labelled Affimer in solution was removed via a two-step centrifugation wash process, applying a relative centrifugal force of 300*g* for 10 min, PBS (pH 7.4) was used as the wash buffer. Prior work showed this method to significantly reduce the background fluorescence level whilst preserving the MB population for use. MB samples were imaged as described above using bright field microscopy, typical post-wash concentrations were in the range of 1–7 × 10^8 mL^{-1} with an average sizing of 2.5 ± 0.3 μm. MB samples were diluted to a concentration of 1 × 10^8 MB mL^{-1} for use on-chip.

2.11. Affimer – microbubble (and Affimer – bead) interactions with biofilms

Following biofilm cultivation and live/dead staining, the biofilms were washed for 5 min with HEPES buffer (150 mM NaCl 50 mM HEPES, pH 7.4) to remove any unbound fluorescent stain. A flow rate of 250 μL min^{-1} was used in all subsequent steps. MB (or beads) suspended in phosphate buffer were flowed into the chamber being tested at a concentration of 1 × 10^8 mL^{-1}, the confocal microscope was used to observe the passage of the particles under investigation into the chamber. The flow was then stopped for 10 min, to allow MB binding to the biofilm, in an inverted chamber. The chamber was then re-orientated and washed with phosphate buffer for 30 min. The inversion step was omitted for bead experiments, which have approximately the same density as water. The flow was stopped during imaging and z-stacks acquired using CLSM. Fig. 2A shows a schematic of the microfluidic platform used, isolation of each chamber was controlled via off-chip valves.

Z-stack image sets (35 slices measuring 30 μm) were acquired at 20 positions within the growth chambers for bead experiments, and 15 positions for MB experiments. The number of image sets taken was

reduced to decrease the acquisition time to reduce the likelihood of MB loss due to dissolution effects, or as a result of toxin release from bacterial cells. The dimensions of each z-stack were converted into an area and the number of MBs/beads per unit area was determined using ImageJ (FIJI) [61]. Bright-field and Alexa Fluor 647 fluorescence channel images were compared throughout the z-stack series to confirm the attachment of MBs/beads. 3D z-stack projections were compiled using LAS X software (Leica, Wetzlar, Germany) and z-stack slices were analyzed using ImageJ. The images for these z-stacks can be found in the raw data repository (DOI: 10.5518/774).

MB samples were diluted to a concentration of 1×10^8 mL^{-1} before use to match the concentration of polystyrene beads used in previous experiments, their size distribution and concentration after washing are shown in Figure SI4. Before injection of the MBs, the microfluidic chip was inverted so that the glass side was facing upwards (inversion of Fig. 2B). AClfA1-MBs and AAC-MBs were then flowed into the microfluidic device and once the MB bolus (1 mL) reached the chamber, the flow was stopped, and the setup incubated at room temperature for 10 min. The microfluidic chip was flipped to its original orientation and flow was resumed to remove any loosely or unbound MBs.

2.12. Biofilm viability and analysis

Biofilm viability was assessed using a bacterial viability kit (*Bac*-Light™, ThermoFisher Scientific, Waltham, MA, USA) prepared by combining 1.5 μL of SYTO™ 9 and propidium iodide (PI) stain components with 1 mL of 0.22 μm filtered 0.8% NaCl solution. This was incubated for 20 min with the biofilm before being washed with HEPES buffer for 10 min (250 μL/min, ~90 refreshes of the device) to remove excess stain. CLSM imaging was performed using a 100 × objective. In all cases, the central chamber of the device was imaged as a control, with US/tMB/US + tMB applied to the side chambers.

A first round of imaging was performed at time T_0 at 10 locations in each chamber within an area that could be covered by the US beam. This set of initial locations were chosen based on notable markers nearby which ensured that the same positions could be re-found and accurately re-aligned during the second round of imaging (T_1). After US exposure, biofilms were re-stained following the same protocol described above to highlight changes in the viability between image sets obtained at T_0 and T_1. Imaging performed at T_1 (after treatment) was performed in the same locations as before to allow direct comparisons to be made. The elapsed time of experiments was approximately 4–5 h, as measured from the start of the first stain until the final image had been taken.

The live and dead cells visible in fluorescent images were counted manually by overlaying a grid and counting cells in each 12 μm × 12 μm square. The cell counts across all grid squares were summed to give a total cell count for the image. Manual counting was checked in a double blind method on sets of images in different treatment types and were found to be within 10% of each other. The count values were deemed to be not accurate to more than 10%.

The dead cell counts (PI stained) were subtracted from the live + dead (SYTO™ 9 stained) cell counts to give separate live and dead cell populations. Changes in the control chamber were counted and used to account for any spontaneous biofilm changes over time. To identify the effectiveness of the different experimental conditions, a fractional change value was calculated for live and dead cell counts for each experimental condition (including the control) ($T_{0,\ LIVE/DEAD} - T_{1,\ LIVE/DEAD}/T_{0,\ TOTAL}$). This value was calculated for each T_0 and T_1 image pair taken at identical imaging positions. The fractional changes in values were then averaged for the 10 imaged locations and an intra-experimental error was calculated. This was repeated for 3 separate experiments and inter-experimental errors estimated. A student's unpaired *t*-test was used for statistical analysis between the different experimental conditions. No statistical differences were identified between first and final locations within the same biofilms, this ruled out cytotoxicity effects contributing to the observed cell death.

2.13. Ultrasound exposure and microbubble destruction

MBs were flowed onto the microfluidic device, incubated, and washed as described above. Following initial imaging, the test chambers were exposed to a 22-cycle sine wave 2.25 MHz signal with a peak negative pressure of 0.8 MPa (MI of 0.54) at a pulse repetition frequency of 10 kHz, for a total duration of 2 s using a single element ultrasound transducer (V323-SM, Olympus, Tokyo, Japan). Fig. 2B shows a schematic of the microfluidic device set-up for the application of US and high magnification CLSM imaging. US was applied at 90° to the device to ensure accuracy in the delivery of US and avoid signal interfering with neighboring chambers. The signal was produced using a signal generator (TG5011, TTI, Fort Worth, TX, USA) controlled by MATLAB (R2019b, The Mathworks Inc, Natick, MA, USA). The duty cycle throughout this pulse sequence was ~1%, checked using an oscilloscope (Waverunner, LeCroy, Chestnut Ridge, NY, USA) and passed through a +53 dB RF amplifier (A150, E&I, Rochester, NY, USA). The *in vitro* signal calibration using a pre-amplified input voltage of 400 mV_{pp} yielded a mechanical index of 0.54 after passage through a 1 mm thick sample of PDMS (as used for the microfluidic devices). Standing waves did not present issues in relation to MB destruction and l was shown to successfully destroy >90% of MBs in a sample within a microfluidic device (Figure SI5).

3. Results

3.1. Production of *S. aureus* biofilm under flow conditions

S. aureus biofilms were grown in microfluidic devices (Figs. 2A, 2B, SI1) at 37 °C under flow conditions chosen to mimic the situation in intravascular infections such as infective endocarditis, where biofilms grow in the bloodstream. A flow rate of 80 μL min^{-1} was used during the growth phase with wash and MB injection flow rates of 250 μL min^{-1} [53, 62]. Fig. 2C shows a CLSM fluorescent image of a typical biofilm, grown for 24 h. The cell density shown in Fig. 2D was similar to that found across all three chambers, with lawn-like growths accompanied by larger projecting 3D structures of variable shape/size, as also found by others [63,64].

3.2. Affimer screening and selection

An Affimer phage display library was screened against biotinylated ClfA/ySUMO protein onto streptavidin-coated microwells to isolate specific binders. After three rounds of panning, 48 randomly picked clones were tested for binding ClfA/ySUMO as well as ySUMO using phage ELISA (Figure SI3). Clones that confirmed binding to ClfA/ySUMO, but not ySUMO, were sent for sequencing. Sequence analysis revealed 16 unique ClfA specific Affimer clones. Additional screening of these Affimer proteins against *S. aureus* biofilms led to the Affimer designated AClfA1 being selected for further investigation.

3.3. Characterization of the binding kinetics of AClfA1 to clumping factor A (ClfA)

Isothermal titration calorimetry (ITC) was used to assess the binding of AClfA1 and AAC against the clumping factor A (ClfA) target. The equilibrium dissociation constant, K_D, gives an indication of binding affinity [65,66]. The interaction between AClfA1 and its target (ClfA) is shown by the steep curve in Fig. 3A. This reaction gave a dissociation constant (K_D) of 62 ± 3 nM, suggesting a high binding affinity. In contrast, no binding was observed between the control AAC and ClfA, as indicated by the flat line in Fig. 3B. As a result of this, a K_D value could not be calculated for AAC. This result indicates that the interaction between AClfA1 and ClfA is specific to the hypervariable loops in the AClfA1 protein structure.

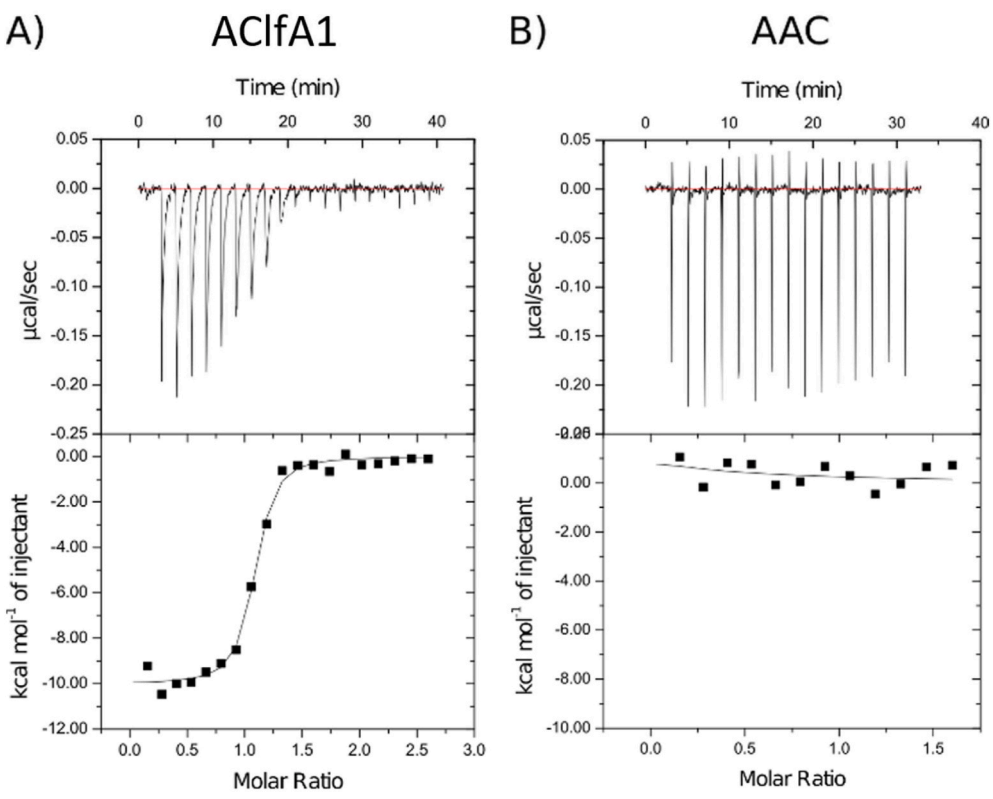

Fig. 3. Isothermal titration calorimetry analysis of AClfA1 and AAC binding to clumping factor A (ClfA). *Top traces* show the heat flow per injection pulse over time. The raw data are the difference in power supplied to the sample and reference cell to maintain isothermal conditions. *Lower traces* show the integrated heat change as a function of Affimer addition. The molar ratio is defined as the [Affimer]/[protein] ratio. A) Titration of Affimer AClfA1 into ClfA. B) Titration of Affimer AAC into ClfA.

3.4. AClfA1 and AAC functionalized micro-bead binding to biofilms

AClfA1 and AAC, labelled with Alexa Fluor A647, were attached to 2 µm polystyrene beads (micromod Partikeltechnologie GmbH, Rostock, Germany) and flowed through microfluidic chambers containing *S. aureus* biofilm. Images were obtained via CLSM, and the number of beads bound to the biofilm surface was counted manually, as described in the methods. The concentration of beads bound to the biofilm per unit

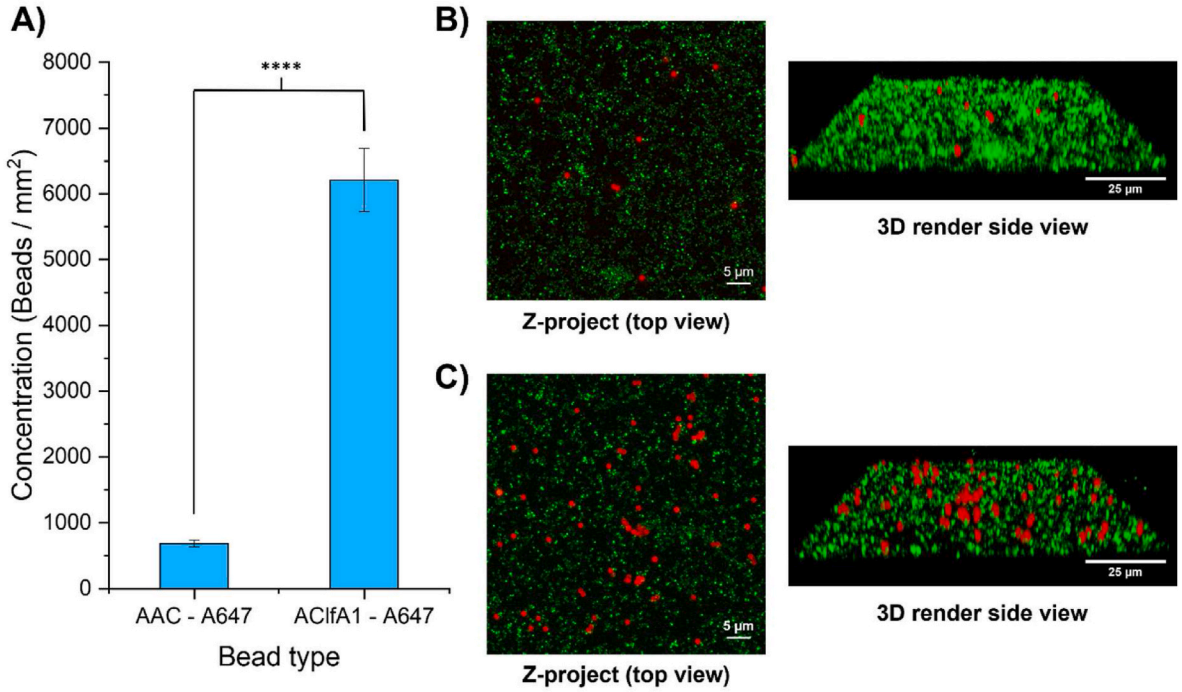

Fig. 4. A) Bar graph showing the mean number of beads per mm^2 for AClfA1 and AAC conjugated 2 µm polystyrene beads, bound to *S. aureus* (UAMS-1) biofilms, after washing with buffer for 30 min to remove unbound particles. Error bars show the standard error obtained from n = 60 images per bead type obtained from three experimental repeats (20 images per repeat). P values indicate: ****≤0.0001. B) Beads conjugated with Affimer AAC-A647. C) Beads conjugated with AClfA1-A647. The green signal shows bacterial cells stained with DMAO™, and the red signal shows beads with Alexa Fluor 647-labelled Affimer attached to their surface. (For interpretation of the references to colour in this figure legend, the reader is referred to the Web version of this article.)

area (Fig. 4) was significantly higher ($P \leq 0.0001$) for AClfA1 (6211 ± 426 beads mm^{-2}), compared to the control AAC (684 ± 99 beads mm^{-2}).

3.5. AClfA1 and AAC functionalized MB binding to biofilms

AClfA1 and AAC were attached to lipid-coated MBs, consisting of DPPC: DSPE–PEG2000–Maleimide (95:5) shell and a C_4F_{10} gas core, and are referred to as targeted MB (tMB) and control MB (cMB) respectively. Fig. 5A shows a significant increase in tMB binding (1390 ± 45 MB mm^{-2}) to *S. aureus* biofilm. Fig. SI 6 shows the spread of binding data for both MBs and beads decorated with AClfA1 or AAC.

3.6. Effect of targeted microbubbles and ultrasound exposure on S. aureus biofilms

Ultrasound (US) induced cavitational effects are known to porate mammalian cells and lead either directly to cell death, or indirectly via enhanced therapeutic uptake [25,43,67,68]. Gram-positive bacteria, however, have an ~60 nm thick bacterial cell wall to protect the cells from lysis and osmotic shock. Thus, it was of interest to understand whether the cavitation of bound MBs would also lead to poration of bacteria or whether it would lead to a break-up of the biofilm, or a combination of these. To assess the effect of bursting the tMB, the biofilms were stained with SYTO™ 9 (green, live/dead cells) and PI (red, dead cells) and imaged before treatment of the biofilm (time = T_0) with US. An ultrasound destruction pulse sequence (2 s, 2.25 MHz, 1 kHz PRF, 22 cycle sine wave, mechanical index of 0.54, 1% duty cycle) was used to burst the MB and the remaining biofilm was re-stained with SYTO™ 9 and PI to highlight changes to cell state and biofilm mass (time = T_1). Representative images from such experiments are shown in Fig. 6. From left to right, columns show images for untreated and US with tMB treated biofilms. After a single exposure combining ultrasound with targeted MBs, a 25% reduction in live cell counts was observed associated with removal of biomass and a concomitant 8% increase in dead cell count. As shown in figures SI6 and SI7, biofilms exposed to US alone or targeted MBs alone did not show comparable levels of cell death.

4. Discussion

4.1. Microfluidics for biofilm study

The microfluidic approach to biofilm study offers an improvement over traditional static systems, such as well plates, as they allow better control over the microenvironment and offer a better mimic of the bloodstream environment where infections, such as infective endocarditis, may occur [45]. Furthermore, microfluidic devices may be easily integrated into existing microscopy systems, thereby allowing non-invasive visualization and imaging in real time of reagent-biofilm interactions. The development of a triple chambered device improved experimental throughput compared to single chamber devices used by others [43,62,69]. CFD modelling of the devices ensured a near-identical growth environment in each chamber through careful flow balancing. By further modifying devices to include separate reagent channels leading into the two side chambers, we were able to apply and study different reagents within the system in parallel. Figure SI1 shows the device used and the associated dimensions, and Figure SI2 shows the whole system including other associated components.

4.2. AClfA1 and ClfA binding kinetics

The AClfA1 – ClfA binding strength, 0.62 nM, was of a similar order of magnitude to that found for other proteins and monoclonal antibodies (mAbs) known to bind to *S. aureus* which typically display K_D values in the range of 0.47 nM–10 pM [66,70]. In contrast, the K_D values observed between gram-positive bacteria and vancomycin, an antibiotic

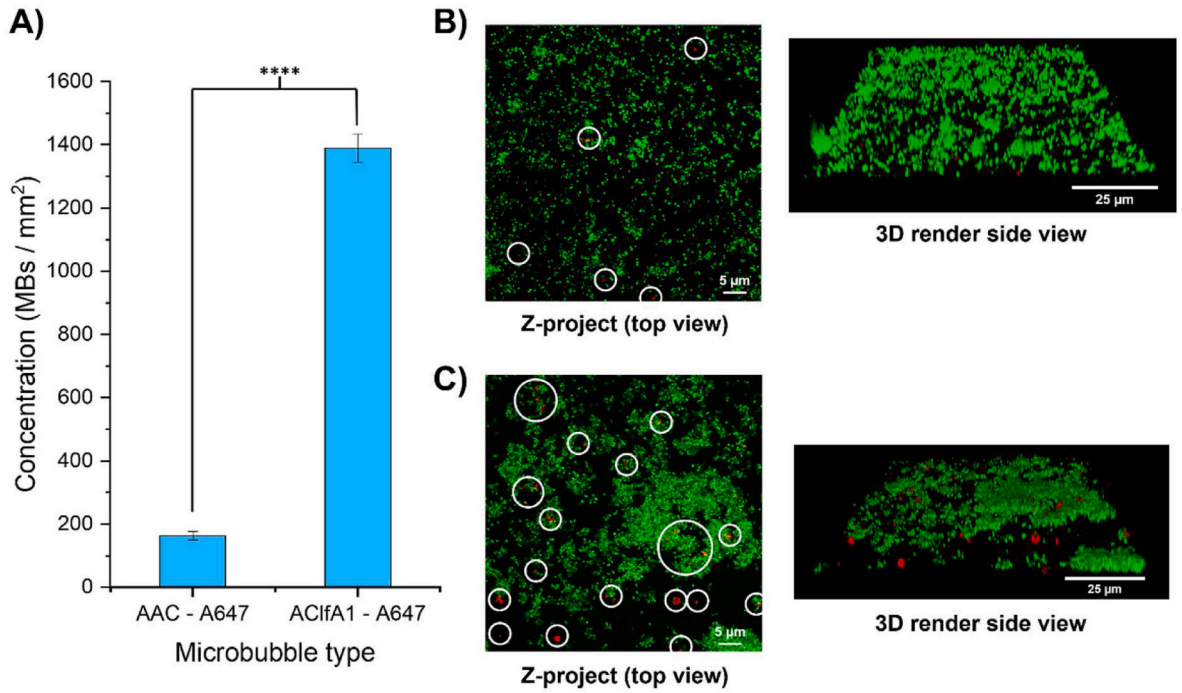

Fig. 5. A) Bar graph showing the average number of MB per mm^2 for AClfA1 and AAC conjugated MBs following incubation with *S. aureus* (UAMS-1) biofilms. Measurements made after washing with phosphate buffer for 30 min to remove unbound MBs. Error bars show the standard error obtained from n = 45 images per MB type obtained from three experimental repeats (15 images per repeat). **** = P value ≤ 0.0001. B) MBs conjugated with AAC-A647. C) MBs conjugated with AClfA1-A647. The green signal shows bacterial cells stained with DMAO™, and red signal, MBs with Alexa Fluor 647-labelled Affimer attached to their surface. White circles have been added to highlight areas of MB attachment. (For interpretation of the references to colour in this figure legend, the reader is referred to the Web version of this article.)

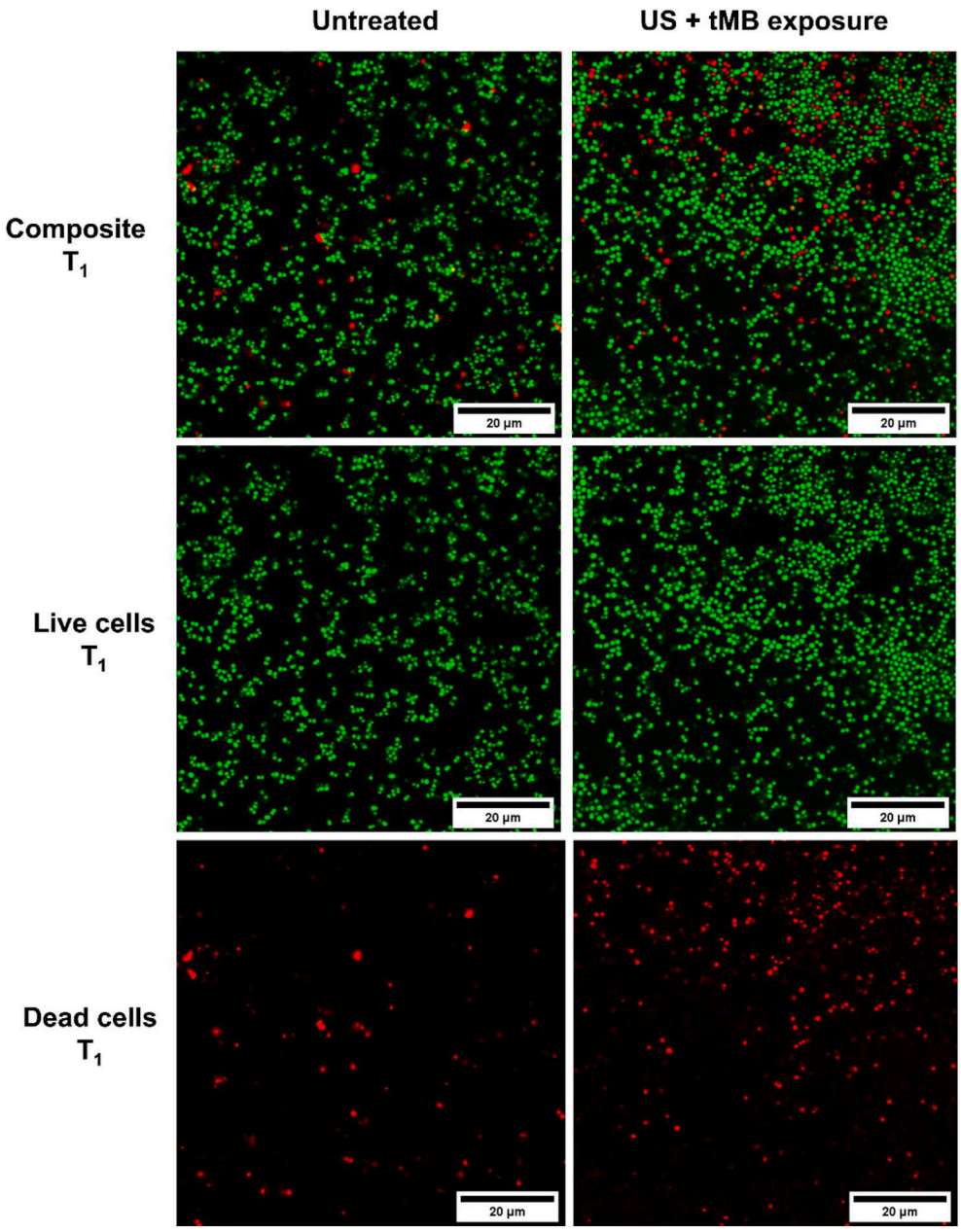

Fig. 6. Representative CLSM image slices of *S. aureus* biofilm grown for 24 h, obtained using a 100 × objective, for untreated (column 1) and US with tMB treated (column 2) samples. Rows 1–3 show composite fluorescence, SYTO™ 9 (green, live/dead) fluorescence only, and propidium iodide (PI) (red, dead cells) fluorescence only, respectively. Scale bars show a distance of 20 μm. (For interpretation of the references to colour in this figure legend, the reader is referred to the Web version of this article.)

commonly used in the treatment of serious infections such as MRSA, ranged from 100 to 1 μM, suggesting that the AClfA1 offers a stronger binding affinity than vancomycin as used by others [41,71]).

4.3. AClfA1 and AAC binding when conjugated to beads and microbubbles

The approximate 9-fold increase in bead concentration at the biofilm surface mediated by AClfA1 coated beads confirmed that the binding interaction was strong enough to anchor 'carrier' particles to the biofilm and withstand an estimated flow-induced shear stress of 0.072 N m^{-2} at a flow rate of 250 μL min^{-1}.

We noted an approximately 5-fold decrease in the number of tMB attached to the surface compared to their bead counterparts, ~1390 ± 45 MB mm^{-2} compared to 6211 ± 426 microbeads mm^{-2}. Figure SI6 shows the spread of bead (A) or MB (B) counts found for each z-stack image series in an imaging area of approximately 116 μm × 116 μm. The typical length of time the biofilm/MB interactions were studies for was ~2–3 h. Hence, we ascribed these differences potentially to i) intrinsic finite lifetime of MBs, ii) reduction in MBs reaching the target sites due to MB destruction during injection into the microfluidics system, and iii) the increased complexity of the experimental method required to enhance MB/biofilm interactions (e.g. chamber inversion process) [58]. Despite the difference in absolute counts, both Figs. 4A and 5A show a comparable ~9-fold increase in the AClfA1 tMBs/beads compared to the non-targeted AAC control isotypes.

4.4. Effect of microbubble destruction on biofilm viability

We observed a ~25% reduction in the number of live cells residing in the biofilm following exposure to tMBs with US. In comparison, *He* et al., and *Agarwal* et al., who also utilized MB destruction, observed biofilm biomass reductions of 25–79% [68,72] In the first study, MBs were applied at concentrations of up to 5 × 10^8/mL, with US applied at 80 kHz using duty cycles up to 100%. In the second study, a continuous perfusion of MBs was applied for 15 min with 2 s US exposures every 2

min.

Others studies have indicated that stable cavitation of MBs may offer a better path towards biomass removal. These investigations demonstrated biofilm biomass or surface clearance of ~15–60% [41,42,44,68,73]. These studies differed in numerous aspects including, i) growth setup (well plates, opticell plates, ibidi chips) ii) delivered US power, mechanical index, and exposure duration, and iii) MB concentration. It is possible that stable cavitation when combined with monodisperse MBs, rather than poyldisperse MBs, may improve biofilm removal further [74–77].

Differences in the quantification methods used in these studies, including crystal violet staining and CFU counting, may also contribute to differences in the perceived effectiveness of treatments. In addition to the removal of ~25% of the biofilm mass we also saw an increase in the residual dead cell count of ~8% as indicated by the increase in PI uptake compared to the various controls (Fig. 6 and Figure SI7 and SI8). Whilst not the focus of this proof-of-principle Affimer targeting study, biofilm removal and bacterial cell death may both be enhanced using targeted MBs over untargeted MBs and could potentially be optimized in the future [42,44,68,73]. Complementary quantification methods such as CFU counting were considered to reaffirm the biomass removal data. However, such methods were considered to be incompatible with the microfluidic system used here.

4.5. Limitations of the study

We have examined biofilms under flow conditions with the specific aim of examining bound MB behavior under flow, rather than using flow to influence biofilm formation per se. This is because the proposed tMB would be injected into the bloodstream and would interact with any intravascular biofilm under conditions of flow. A simple *in vitro* model cannot replicate the wide variation in flow rates and shear forces that occur throughout the cardiac cycle and within the different elements of the human vasculature, particularly in patients with heart valve disease and/or bloodstream infection. In the setting of infective endocarditis where vegetations are usually found on heart valves or intracardiac devices, the blood flow rate will be approximately the same as blood flow through the heart, but will be variable around abnormal anatomy and devices. Hence, shear forces in these regions will also be highly variable. We estimated the shear forces likely to be produced in our model to allow comparison with other studies. Although this work provides proof of principle that tMB can bind *S. aureus* biofilms and withstand some degree of shear force, it is likely that an animal model of infective endocarditis would be needed to test the performance of tMB in the varied flow conditions that occur *in vivo*. Testing the behavior of bound tMB under higher flow rates was not possible because higher flow rates caused biofilm detachment. Testing at lower flow rates was prevented by blockages that formed at lower flow rates.

This study has focused on attachment to a single *S. aureus* strain and it cannot be assumed that the UAMS-1 strain used here is representative of all *S. aureus* strains. We are currently investigating the affinity of the tMBs of this study against a range of other *S. aureus* strains and bacterial species. Further investigations are also being conducted to measure the binding affinity of a multitude of other novel Affimer proteins that were identified alongside AClfA1. Finally, the methods used to assess the changes in biofilm viability following different exposure types could be further improved to reduce the observed variability. Future studies will incorporate several different approaches to assess the response of biofilms to different exposure types. These methods could include a combination of growth environments so that bacterial counting, biomass staining, and live/dead staining could all be applied.

5. Conclusions

This work has identified a novel Affimer protein, AClfA1, which can provide a strong level of binding ($K_D = 62 \pm 3$ nM) against clumping factor A, a virulence factor expressed by *S. aureus*. We have demonstrated that surface functionalization of "carrier" particles, namely polystyrene beads and lipid-coated MBs showed improved binding to *S. aureus* (UAMS-1) biofilms by 8–10 times, as compared to a control Affimer protein, AAC. Finally, we demonstrated that the US induced destruction of biofilm-bound tMBs leads i) removal of biofilm and ii) poration of the bacterial cell wall and cell death. However, this requires optimization before being considered a biomechanical method of biofilm treatment or to be used in combination with drugs to improve treatment. Clinical use of this approach would likely involve co-delivery of antimicrobial agents to improve treatment efficacy, as suggested by others [43,45,68].

Funding

EPSRC (EP/1000623, EP/K023845), NIHR (MIC-2016-004), BBSRC (BB/M005666/1), Wellcome Trust (094232/Z/10/Z).

Data availability statement

The datasets generated for this study can be found in the University of Leeds data repository, available at https://doi.org/10.5518/774.

CRediT authorship contribution statement

Jack A. Caudwell: performed experimental work, Formal analysis, Writing – original draft, ‡ these authors contributed equally. **Jordan M. Tinkler:** performed experimental work, Formal analysis, Writing – original draft, ‡ these authors contributed equally. **Ben R.G. Johnson:** helped with experimental setup design, fabrication of components, Writing – original draft. **Kenneth J. McDowall:** performed the initial identification and isolation of the Affimer proteins used in this work, Writing – original draft. **Fayez Alsulaimani:** performed the initial identification and isolation of the Affimer proteins used in this work, Writing – original draft. **Christian Tiede:** performed the initial identification and isolation of the Affimer proteins used in this work, Writing – original draft. **Darren C. Tomlinson:** performed the initial identification and isolation of the Affimer proteins used in this work, Writing – original draft. **Steven Freear:** Conceptualization, Project administration, interpretation, Writing – original draft, gave approval to the final version of the manuscript. **W. Bruce Turnbull:** Conceptualization, Project administration, interpretation, Writing – original draft, gave approval to the final version of the manuscript. **Stephen D. Evans:** Conceptualization, Project administration, interpretation, Writing – original draft, gave approval to the final version of the manuscript. **Jonathan A.T. Sandoe:** Conceptualization, Project administration, interpretation, Writing – original draft, gave approval to the final version of the manuscript.

Declaration of competing interest

The authors declare that the research was conducted in the absence of any commercial or financial relationships that could be construed as a potential conflict of interest.

Acknowledgments

The authors would like to thank Damien Bachelor for work on MATLAB coding scripts used for bubble populations counting and US exposure control, and members from the Microbubble Consortium (https://microbubbles.leeds.ac.uk/) for their help and insights. Special thanks are owed to Dr Peyman for contributions towards the development of microfluidics used throughout this work. JC was funded by University of Leeds Anniversary Research Scholarship (LARS), JT was funded with Alumni support and the University of Leeds funding, and FA was funded by King Abdulaziz University and the Ministry of Higher

Education, Saudi Arabia. We also acknowledge the EPSRC for their contributions towards the microbubble work (EP/1000623, EP/K023845) and SDE acknowledges support through NIHR (MIC-2016-004). We also thank BBSRC for support for the protein engineering work (BB/M005666/1) and The Wellcome Trust for funds for the iTC200 (094232/Z/10/Z). A final thanks is owed to the University of Leeds Innovation funding. The data used in the figures of this paper are available at https://doi.org/10.5518/774.

Appendix A. Supplementary data

Supplementary data to this article can be found online at https://doi.org/10.1016/j.bioflm.2022.100074.

References

[1] Ribas, V.J., López, J.C., Ruiz-Rodriguez, J.C., Rello, J., Wojdel, A., and Vellido, A. (Year). "Severe sepsis mortality prediction with relevance vector machines", in: *33rd Annual International Conference of the IEEE EMBS*).

[2] de Oliveira TH, Amorin AT, Rezende IS, Santos Barbosa M, Martins HB, Brito AK, et al. Sepsis induced by Staphylococcus aureus: participation of biomarkers in a murine model. Med Sci Mon Int Med J Exp Clin Res 2015;21:345–55. https://doi.org/10.12659/MSM.892528.

[3] Paulsen J, Mehl A, Askim A, Solligard E, Asvold BO, Damas JK. Epidemiology and outcome of Staphylococcus aureus bloodstream infection and sepsis in a Norwegian county 1996-2011: an observational study. BMC Infect Dis 2015;15:116. https://doi.org/10.1186/s12879-015-0849-4.

[4] Moormeier DE, Bayles KW. Staphylococcus aureus biofilm: a complex developmental organism. Mol Microbiol 2017;104(3):365–76. https://doi.org/10.1111/mmi.13634.

[5] Kourtis AP, Hatfield K, Baggs J, Mu Y, See I, Epson E, et al. *Vital signs*: epidemiology and recent trends in methicillin-resistant and in methicillin-susceptible *Staphylococcus aureus* bloodstream infections - United States. In: *MMWR Morbidity and mortality weekly report* US Department of Health and human services/centers for disease control and prevention); 2019.

[6] Cai YM. Non-surface attached bacterial aggregates: a ubiquitous third lifestyle. Front Microbiol 2020;11:557035. https://doi.org/10.3389/fmicb.2020.557035.

[7] Flemming HC, Wingender J. The biofilm matrix. Nat Rev Microbiol 2010;8(9):623–33. https://doi.org/10.1038/nrmicro2415.

[8] Paharik AE, Horswill AR. The staphylococcal biofilm: adhesins, regulation, and host response. Microbiol Spectr 2016;4(2). https://doi.org/10.1128/microbiolspec.VMBF-0022-2015.

[9] Aka ST, Haji SH. Sub-MIC of antibiotics induced biofilm formation of Pseudomonas aeruginosa in the presence of chlorhexidine. Braz J Microbiol 2015;46(1):149–54. https://doi.org/10.1590/S1517-838246120140218.

[10] Sharma D, Misba L, Khan AU. Antibiotics versus biofilm: an emerging battleground in microbial communities. Antimicrob Resist Infect Control 2019;8:76. https://doi.org/10.1186/s13756-019-0533-3.

[11] Bowler P, Murphy C, Wolcott R. Biofilm exacerbates antibiotic resistance: is this a current oversight in antimicrobial stewardship? Antimicrob Resist Infect Control 2020;9(1):162. https://doi.org/10.1186/s13756-020-00830-6.

[12] Gould FK, Denning DW, Elliott TS, Foweraker J, Perry JD, Prendergast BD, et al. Guidelines for the diagnosis and antibiotic treatment of endocarditis in adults: a report of the Working Party of the British Society for Antimicrobial Chemotherapy. J Antimicrob Chemother 2012;67(2):269–89. https://doi.org/10.1093/jac/dkr450.

[13] Baddour LM, Wilson WR, Bayer AS, Fowler Jr VG, Tleyjeh IM, Rybak MJ, et al. Infective endocarditis in adults: diagnosis, antimicrobial therapy, and management of complications: a scientific statement for healthcare professionals from the American heart association. Circulation 2015;132(15):1435–86. https://doi.org/10.1161/CIR.0000000000000296.

[14] Grant CA, McKendry JE, Evans SD. Temperature dependent stiffness and visco-elastic behaviour of lipid coated microbubbles using atomic force microscopy. Soft Matter 2012;8(5):1321–6. https://doi.org/10.1039/c1sm06578e.

[15] Jangjou A, Meisami AH, Jamali K, Niakan MH, Abbasi M, Shafiee M, et al. The promising shadow of microbubble over medical sciences: from fighting wide scope of prevalence disease to cancer eradication. J Biomed Sci 2021;28(1):49. https://doi.org/10.1186/s12929-021-00744-4.

[16] de Jong N, Bouakaz A, Frinking P. Basic acoustic properties of microbubbles. Echocardiography 2002;19(3):229–40. https://doi.org/10.1046/j.1540-8175.2002.00229.x.

[17] Hauff P, Reinhardt M, Foster S. Ultrasound contrast agents for molecular imaging. In: Semmler W, Schwaiger M, editors. Molecular imaging I. Handbook of experimental pharmacology. Springer Berlin Heidelberg; 2008. p. 223–45.

[18] Sirsi S, Borden M. Microbubble compositions, properties and biomedical applications. Bubble Sci Eng Technol 2009;1(1–2):3–17. https://doi.org/10.1179/175889709X446507.

[19] Faez T, Goertz D, De Jong N. Characterization of Definity ultrasound contrast agent at frequency range of 5-15 MHz. Ultrasound Med Biol 2011;37(2):338–42. https://doi.org/10.1016/j.ultrasmedbio.2010.11.014.

[20] Jarvis S. Vascular system 1: anatomy and physiology. Nurs Times 2018;114(4):40–4.

[21] Weller GER, Klibanov AL, Wong MKK, Wagner WR, Modzelewski RA, Lu E, et al. Ultrasonic imaging of tumor angiogenesis using contrast microbubbles targeted via the tumor-binding peptide Arginine-Arginine-leucine. Cancer Res 2005;65(2).

[22] Willmann JK, Lutz AM, Paulmurugan R, Patel MR, Chu P, Rosenberg J, et al. Dual-targeted contrast agent for US assessment of tumor angiogenesis in vivo. Radiology 2008;248(3).

[23] Anderson CR, Rychak JJ, Backer M, Backer J, Ley K, Klibanov AL. scVEGF microbubble ultrasound contrast agents: a novel probe for ultrasound molecular imaging of tumor angiogenesis. Invest Radiol 2010;45(10):579–85. https://doi.org/10.1097/RLI.0b013e3181efd581.

[24] Anderson CR, Hu X, Zhang H, Tlaxca J, Declèves AE, Robert Houghtaling r, et al. Ultrasound molecular imaging of tumor angiogensis with an integrin targeted microbubble contrast agent. Invest Radiol 2011;46(4).

[25] Kooiman K, Foppen-Harteveld M, van der Steen AFW, de Jong N. Sonoporation of endothelial cells by vibrating targeted microbubbles. J Contr Release 2011;154:35–41. https://doi.org/10.1016/j.jconrel.2011.04.008.

[26] Park YC, Zhang C, Kim S, Mohamedi G, Beigie C, Nagy JO, et al. Microvessels-on-a-Chip to assess targeted ultrasound-assisted drug delivery. ACS Appl Mater Interfaces 2016;8(46):31541–9. https://doi.org/10.1021/acsami.6b09071.

[27] van Rooij T, Skachkov I, Beekers I, Lattwein KR, Voorneveld JD, Kokhuis TJA, et al. Viability of endothelial cells after ultrasound-mediated sonoporation: influence of targeting, oscillation, and displacement of microbubbles. J Contr Release 2016;238:197–211. https://doi.org/10.1016/j.jconrel.2016.07.037.

[28] Skachkov I, Luan Y, van Tiel ST, van der Steen AFW, de Jong N, Bernsen MR, et al. SPIO labeling of endothelial cells using ultrasound and targeted microbubbles at diagnostic pressures. PLoS One 2018;13(9):e0204354. https://doi.org/10.1371/journal.pone.0204354.

[29] Ingels A, Leguerney I, Cournede PH, Irani J, Ferlicot S, Sebrie C, et al. Ultrasound molecular imaging of renal cell carcinoma: VEGFR targeted therapy monitored with VEGFR1 and FSHR targeted microbubbles. Sci Rep 2020;10(1):7308. https://doi.org/10.1038/s41598-020-64433-2.

[30] Li T, Hu Z, Wang C, Yang J, Zeng C, Fan R, et al. PD-L1-targeted microbubbles loaded with docetaxel produce a synergistic effect for the treatment of lung cancer under ultrasound irradiation. Biomater Sci 2020;8(5):1418–30. https://doi.org/10.1039/c9bm01575b.

[31] Liu H, Gao M, Gu J, Wan X, Wang H, Gu Q, et al. VEGFR1-Targeted contrast-enhanced ultrasound imaging quantification of vasculogenic mimicry microcirculation in a mouse model of choroidal melanoma. Transl Vis Sci Technol 2020;9(3):4. https://doi.org/10.1167/tvst.9.3.4.

[32] Pochon S, Tardy I, Bussat P, Bettinger T, Brochot J, von Wronski M, Passantino L, Schneider M. BR55: a lipopeptide-based VEGFR2-targeted ultrasound contrast agent for molecular imaging of angiogenesis. Invest Radiol 2010;45(2):89–95.

[33] Warram, J.M., Sorace, A.G., Saini, R., Umphrey, H.R., Zinn, K.R., and Hoyt, K. (20111). A triple-targeted ultrasound contrast agent provides improved localization to tumor vasculature. J Ultrasound Med. 30(7).

[34] Lindner JR, Song J, Xu F, Klibanov AL, Singbartl K, Ley K, et al. Noninvasive ultrasound imaging of inflammation using microbubbles targeted to activated leukocytes. Circulation 2000;102.

[35] Rychak JJ, Lindner JR, Ley K, Klibanov AL. Deformable gas-filled microbubbles targeted to P-selectin. J Contr Release 2006;114(3):288–99. https://doi.org/10.1016/j.jconrel.2006.06.008.

[36] Yeh JS, Sennoga CA, McConnell E, Eckersley R, Tang MX, Nourshargh S, et al. A targeting microbubble for ultrasound molecular imaging. PLoS One 2015;10(7):e0129681. https://doi.org/10.1371/journal.pone.0129681.

[37] Owen J, Rademeyer P, Chung D, Cheng Q, Holroyd D, Coussios C, et al. Magnetic targeting of microbubbles against physiologically relevant flow conditions. Interface Focus 2015;5(5):20150001. https://doi.org/10.1098/rsfs.2015.0001.

[38] Owen J, Crake C, Lee JY, Carugo D, Beguin E, Khrapitchev AA, et al. A versatile method for the preparation of particle-loaded microbubbles for multimodality imaging and targeted drug delivery. Drug Deliv Transl Res 2018;8(2):342–56. https://doi.org/10.1007/s13346-017-0366-7.

[39] de Saint Victor M, Barnsley LC, Carugo D, Owen J, Coussios CC, Stride E. Sonothrombolysis with magnetically targeted microbubbles. Ultrasound Med Biol 2019;45(5):1151–63. https://doi.org/10.1016/j.ultrasmedbio.2018.12.014.

[40] Anastasiadis P, Mojica KDA, John S Allen JS, Matter ML. Detection and quantification of bacterial biofilms combining high-frequency acoustic microscopy and targeted lipid microparticles. J Nanobiotechnol 2014;12(24). https://doi.org/10.1186/1477-3155-12-24.

[41] Kouijzer JJP, Lattwein KR, Beekers I, Langeveld SAG, Leon-Grooters M, Strub JM, et al. Vancomycin-decorated microbubbles as a theranostic agent for Staphylococcus aureus biofilms. Int J Pharm 2021;121154. https://doi.org/10.1016/j.ijpharm.2021.121154.

[42] Dong Y, Chen S, Wang Z, Peng N, Yu J. Synergy of ultrasound microbubbles and vancomycin against Staphylococcus epidermidis biofilm. J Antimicrob Chemother 2013;68(4):816–26. https://doi.org/10.1093/jac/dks490.

[43] Ronan E, Edjiu N, Kroukamp O, Wolfaardt G, Karshafian R. USMB-induced synergistic enhancement of aminoglycoside antibiotics in biofilms. Ultrasonics 2016;69:182–90. https://doi.org/10.1016/j.ultras.2016.03.017.

[44] Dong Y, Xu Y, Li P, Wang C, Cao Y, Yu J. Antibiofilm effect of ultrasound combined with microbubbles against Staphylococcus epidermidis biofilm. Int J Med Microbiol 2017;307(6):321–8. https://doi.org/10.1016/j.ijmm.2017.06.001.

[45] Lattwein KR, Shekhar H, van Wamel WJB, Gonzalez T, Herr AB, Holland CK, et al. An in vitro proof-of-principle study of sonobactericide. Sci Rep 2018;8(1):3411. https://doi.org/10.1038/s41598-018-21648-8.

[46] Vazquez-Lombardi R, Phan TG, Zimmermann C, Lowe D, Jermutus L, Christ D. Challenges and opportunities for non-antibody scaffold drugs. Drug Discov Today 2015;20(10):1271–83. https://doi.org/10.1016/j.drudis.2015.09.004.
[47] Berman HM, Henrick K, Nakamura H. Announcing the worldwide protein data bank. Nat Struct Biol 2003;10(12).
[48] McDevitt D, Francois P, Vaudaux P, Foster TJ. Molecular characterization of the clumping factor (fibrinogen receptor) of *Staphylococcus aureus*. Mol Microbiol 1994;11(2):237–48. https://doi.org/10.1111/j.1365-2958.1994.tb00304.x.
[49] Deivanayagam CC, Wann ER, Chen W, Carson M, Rajashankar KR, Hook M, et al. A novel variant of the immunoglobulin fold in surface adhesins of Staphylococcus aureus: crystal structure of the fibrinogen-binding MSCRAMM, clumping factor A. EMBO J 2002;21(24):6660–72. https://doi.org/10.1093/emboj/cdf619.
[50] Speziale P, Pietrocola G, Foster TJ, Geoghegan JA. Protein-based biofilm matrices in Staphylococci. Front Cell Infect Microbiol 2014;4:171. https://doi.org/10.3389/fcimb.2014.00171.
[51] Sharma AK, Dhasmana N, Dubey N, Kumar N, Gangwal A, Gupta M, et al. Bacterial virulence factors: secreted for survival. Indian J Microbiol 2017;57(1):1–10. https://doi.org/10.1007/s12088-016-0625-1.
[52] Paquet-Mercier F, Parvinzadeh Gashti M, Bellavance J, Taghavi SM, Greener J. Through thick and thin: a microfluidic approach for continuous measurements of biofilm viscosity and the effect of ionic strength. Lab Chip 2016;16(24):4710–7. https://doi.org/10.1039/c6lc01101b.
[53] Becker RC, DiBello PM, Lucas FV. Bacterial tissue tropism: an in vitro model for infective endocarditis. Cardiovasc Res 1987;21:813–20. https://doi.org/10.1093/cvr/21.11.813.
[54] Chavakis T, Wiechmann K, Preissner KT, Herrmann M. Staphylococcus aureus interactions with the endothelium: the role of bacterial "secretable expanded repertoire adhesive molecules" (SERAM) in disturbing host defense systems. Thromb Haemostasis 2005;94(2):278–85. https://doi.org/10.1160/TH05-05-0306.
[55] Tang AA, Tiede C, Hughes DJ, McPherson MJ, Tomlinson DC. Isolation of isoform-specific binding proteins (Affimers) by phage display using negative selection. Sci Signal 2017;10(505). https://doi.org/10.1126/scisignal.aan0868.
[56] Tiede C, Tang AA, Deacon SE, Mandal U, Nettleship JE, Owen RL, et al. Adhiron: a stable and versatile peptide display scaffold for molecular recognition applications. Protein Eng Des Sel 2014;27(5):145–55. https://doi.org/10.1093/protein/gzu007.
[57] Wiseman T, Williston S, Brandts JF, Lin LN. Rapid measurement of binding constants and heats of binding using a new titration calorimeter. Anal Biochem 1989;179:131–7. https://doi.org/10.1016/0003-2697(89)90213-3.
[58] Abou-Saleh RH, Peyman SA, Johnson BR, Marston G, Ingram N, Bushby R, et al. The influence of intercalating perfluorohexane into lipid shells on nano and microbubble stability. Soft Matter 2016;12(34):7223–30. https://doi.org/10.1039/c6sm00956e.
[59] Peyman SA, Abou-Saleh RH, McLaughlan JR, Ingram N, Johnson BR, Critchley K, et al. Expanding 3D geometry for enhanced on-chip microbubble production and single step formation of liposome modified microbubbles. Lab Chip 2012;12(21):4544–52. https://doi.org/10.1039/c2lc40634a.
[60] Batchelor DVB. First public release of MATLAB Microbubble count. 1 ed 2020 (GitHub).
[61] Schindelin J, Arganda-Carreras I, Frise E, Kaynig V, Longair M, Pietzsch T, et al. Fiji: an open-source platform for biological-image analysis. Nat Methods 2012;9(7):676–82. https://doi.org/10.1038/nmeth.2019.
[62] Park A, Jeong HH, Lee J, Kim KP, Lee CS. Effect of shear stress on the formation of bacterial biofilm in a microfluidic channel. BioChip J 2011;5(3):236–41. https://doi.org/10.1007/s13206-011-5307-9.
[63] Moormeier DE, Endres JL, Mann EE, Sadykov MR, Horswill AR, Rice KC, et al. Use of microfluidic technology to analyze gene expression during Staphylococcus aureus biofilm formation reveals distinct physiological Niches. Appl Environ Microbiol 2013;79(11):3413–24.
[64] Moormeier DE, Bose JL, Horswill AR, Baylesa KW. Temporal and stochastic control of Staphylococcus aureus biofilm development. Am Soc Microbiol 2014;5(5).
[65] Fei Y, Sun YS, Li Y, Lau K, Yu H, Chokhawala HA, et al. Fluorescent labeling agents change binding profiles of glycan-binding proteins. Mol Biosyst 2011;7(12):3343–52. https://doi.org/10.1039/c1mb05332a.
[66] Landry JP, Ke Y, Yu GL, Zhu XD. Measuring affinity constants of 1450 monoclonal antibodies to peptide targets with a microarray-based label-free assay platform. J Immunol Methods 2015;417:86–96. https://doi.org/10.1016/j.jim.2014.12.011.
[67] Karshafian R, Bevan PD, Williams R, Amac S, Burns PN. Sonoporation by ultrasound-activated microbubble contrast agents: effect of acoustic exposure parameters on cell membrane permeability and cell viability. Ultrasound Med Biol 2009;35(5):847–60. https://doi.org/10.1016/j.ultrasmedbio.2008.10.013.
[68] He N, Hu J, Liu H, Zhu T, Huang B, Wang X, et al. Enhancement of vancomycin activity against biofilms by using ultrasound-targeted microbubble destruction. Antimicrob Agents Chemother 2011;55(11). https://doi.org/10.1128/AAC.00542-11.
[69] Yawata Y, Toda K, Setoyama E, Fukuda J, Suzuki H, Uchiyama H, et al. Monitoring biofilm development in a microfluidic device using modified confocal reflection microscopy. J Biosci Bioeng 2010;110(3):377–80. https://doi.org/10.1016/j.jbiosc.2010.04.002.
[70] Kangwa M, Yelemane V, Ponnurangam A, Fernandez-Lahore M. An engineered Staphylococcal Protein A based ligand: production, characterization and potential application for the capture of Immunoglobulin and Fc-fusion proteins. Protein Expr Purif 2019;155:27–34. https://doi.org/10.1016/j.pep.2018.11.003.
[71] Yao N, Wu CY, Xiao W, Lam KS. Discovery of high-affinity peptide ligands for vancomycin. Biopolymers 2008;90(3):421–32. https://doi.org/10.1002/bip.20949.
[72] Agarwal A, Ng WJ, Liu Y. Removal of biofilms by intermittent low-intensity ultrasonication triggered bursting of microbubbles. Biofouling 2014;30(3). https://doi.org/10.1080/08927014.2013.876624.
[73] Zhu C, He N, Cheng T, Tan H, Guo Y, Chen D, et al. Ultrasound-targeted microbubble destruction enhances human β-defensin 3 activity against antibiotic-resistant Staphylococcus biofilms. Inflammation 2013;36(5). https://doi.org/10.1007/s10753-013-9630-2.
[74] Doinikov AA. Bjerknes forces and translational bubble dynamics. 2005.
[75] Lazarus C, Pouliopoulos AN, Tinguely M, Garbin V, Choi JJ. Clustering dynamics of microbubbles exposed to low-pressure 1-MHz ultrasound. J Acoust Soc Am 2017;142(5):3135. https://doi.org/10.1121/1.5010170.
[76] LuTheryn G, Glynne-Jones P, Webb JS, Carugo D. Ultrasound-mediated therapies for the treatment of biofilms in chronic wounds: a review of present knowledge. Microb Biotechnol 2020;13(3):613–28. https://doi.org/10.1111/1751-7915.13471.
[77] Vyas N, Wang QX, Manmi KA, Sammons RL, Kuehne SA, Walmsley AD. How does ultrasonic cavitation remove dental bacterial biofilm? Ultrason Sonochem 2020;67:105112. https://doi.org/10.1016/j.ultsonch.2020.105112.